Coherent detection schemes for subcarrier wave continuous variable quantum key distribution

E. SAMSONOV[1,2,3,*], R. GONCHAROV[1,3], M. FADEEV[1], A. ZINOVIEV[1], D. KIRICHENKO[1,3], B. NASEDKIN[1,3], A. D. KISELEV[1,3], AND V. EGOROV[1,2,4]

[1] *Quantum Information Laboratory, ITMO University, Kadetskaya Line, 3, Saint Petersburg, 199034, Russia*
[2] *Quanttelecom LLC, 6th Vasilyevskogo Ostrova Line, 59, Saint Petersburg, 199178, Russia*
[3] *Laboratory of Quantum Processes and Measurements, ITMO University, Kadetskaya Line, 3, Saint Petersburg, 199034, Russia*
[4] *Leading Research Center "National Center of Quantum Internet", ITMO University, Birzhevaya Line, 16, Saint Petersburg, 199034, Russia*
[*] *eosamsonov@itmo.ru*

Abstract: We examine different methods to implement coherent detection in the subcarrier wave quantum key distribution (SCW QKD) systems. For classical wavefields, we present the models describing homodyne-type and heterodyne-type coherent detection schemes needed to extract information from the quadrature phase-coded multimode signals used in SCW QKD. Practical feasibility of the proposed schemes is corroborated by the experiments.

1. Introduction

Since 1896, when the "beat receptor", the first heterodyne detector, as we know it now, was invented by Nicola Tesla [1], various forms of coherent detection methods, including homodyne and heterodyne detection, have found wide use in a variety of applications. Starting with radio communications [2], the coherent detection methods have been expanded to the optical domain [3]. Nowadays there are numerous examples of optical coherent detection usage in different fields including telecommunications [4–8] and quantum optics [9–11]. The quantum key distribution (QKD), which is one of the most active areas in quantum information and represents a promising quantum technology, in combination with coherent detection leads to a separate branch, known as the continuous variable (CV) QKD [12–21]. The CV-QKD systems rely on the methods of coherent detection for gaining information encoded in the electromagnetic field quadratures. In other words, single-photon detection can be replaced by conventional detection methods.

Active development of novel QKD systems utilising modulated multimode states of light necessitates reconsideration and modification of the existing detection schemes. A striking example of such a system is the subcarrier wave (SCW) QKD [22–29]. The method for quantum state encoding is the distinguishing feature of the SCW QKD. In this method, a strong monochromatic wave emitted by a laser is modulated in an electro-optic phase modulator to produce weak sidebands, whose relative phase with respect to the strong (carrier) wave encodes the quantum information (a detailed description of the discrete variable (DV) SCW QKD conventional protocol and the SCW CV-QKD protocol can be found in [24] and [29], respectively).

In this paper we present three coherent detection schemes with phase estimation to demodulate the quadrature phase-coded multimode signals. This type of signals is used to encode quantum information in the SCW QKD systems. The main advantage of the proposed schemes is using the carrier wave which plays a leading part in the SCW methodology as a local oscillator (LO). In practice, it provides an alternative solution of the well-known problem of transmitting the local

oscillator through the quantum channel (or its generation on the receiver's side). This is the novel approach that has not been previously discussed in works on the multimode CV-QKD [30–32]. So we present the theoretical models describing the proposed detection schemes and experimentally demonstrate how to implement coherent detection using the carrier wave as a local oscillator.

2. Phase-coded multimode signals

Our first step is to describe generation of the phase-coded multimode signals that is the essential part of the SCW QKD system. Since our proof-of-principle experiments use classical light, we shall utilise the classical model of electro-optic phase modulation [33]. Note that quantum description of electro-optic modulation applicable to quantum states can be found in [34–36].

As is shown in Figure 1, a monochromatic lightwave with the frequency ω and the amplitude E_0 is modulated by the traveling wave electro-optic phase modulator using the microwave field with the frequency Ω and the phase φ_A [37]. The phase-modulated optical field $E(t)$ then can be expressed in terms of Jacobi–Anger expansion as follows

$$E(t) = E_0 e^{i\omega t} e^{im_A \cos(\Omega t+\varphi_A)} = E_0 e^{i\omega t} \sum_{k=-\infty}^{\infty} i^k J_k(m_A) e^{ik(\Omega t+\varphi_A)}, \tag{1}$$

where $J_k(m_A)$ is the k-order Bessel function of the first kind and m_A is the modulation index which is typically small in the SCW QKD protocols. As a result, the sidebands are formed at the frequencies $\omega_k = \omega + k\Omega$, where k is the integer.

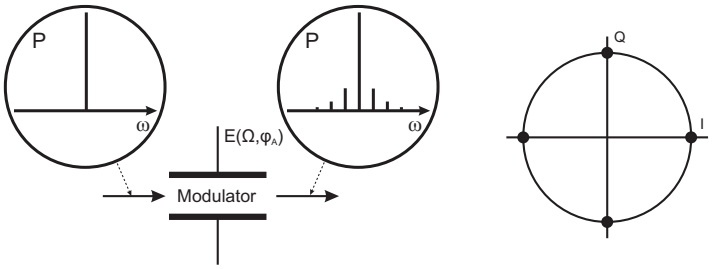

Fig. 1. Modulated light emerging after the electro-optic phase modulator and 4-PSK constellation diagram. The typical power spectrum at the modulator output in SCW QKD is also shown.

The modulated light beam emerging at the output of the phase modulator contains the reference carrier ($k = 0$) and the sidebands ($k \neq 0$). The relative phase and amplitude between reference and all the sidebands are determined by the inner microwave field that controls the phase φ_A and the modulation index m_A, respectively. Therefore one may encode the information into the sidebands of the phase-modulated light by applying different forms of quadrature amplitude modulation [23, 24, 38–40]. In this paper, for simplicity, we concentrate on the quadrature phase-shift keying which is extensively used in CV-QKDs with discrete modulation [18,19,41,42]. We prepare the phase-coded multimode signals by selecting the phase of the microwave field from the finite set of $\varphi_A \in \{0,\ \pi/2,\ \pi,\ 3\pi/2\}$ which is equivalent to the four states commonly used in the CV-QKD protocols with discrete modulation. An example of the modulated signal constellation diagram is presented in Figure 1.

3. Subcarrier wave implementations of coherent detection

3.1. Classical coherent detection

For comparison purposes, we begin with a brief discussion of the basic concepts of coherent detection which is based on using a 50/50 beam splitter to mix an initial weak signal of the power

P_s and the reference field generated by an external source of the power P_{LO} also known as the local oscillator (LO). The mixed optical fields at the outputs of the beam splitter are detected by a photodiode, and the difference between the signals is registered by a balanced detector. It turned out that the output signal whose power is proportional to the square root of LO power, $\sqrt{P_{LO}}$, carries the information about the initial signal. In addition, subtraction of the signals results in reduction of noise components, whereas the amplification scheme installed in the balanced detector is used for further amplification of its response.

In the case of homodyne detection, the signal frequency ω_s and the LO frequency ω_{LO} are equal. The constant signal level that will be observed is determined by the phase difference between the initial signal and the LO, $\Delta\phi = \phi_s - \phi_{LO}$. For instance, when the constant signal on the oscilloscope is positive at zero phase difference, it will be negative provided the phase difference equals π. More precisely, in the absence of noise, the output of the detector is proportional to the difference between the photocurrents registered by the photodiodes and can be written in the following form [6]:

$$I(t) = I_1(t) - I_2(t) = 2R(\lambda)G\sqrt{P_s(t)P_{LO}}\cos\Delta\varphi = 2R(\lambda)GCE_s(t)E_{LO}\cos\Delta\phi, \qquad (2)$$

where $R(\lambda)$ is the responsivity of photodiodes; G is the electronic gain of balanced detector; $C = S/(2\xi)$ is the ratio of the effective beam area S and the doubled impedance ξ of the medium; E_s and E_{LO} are the amplitudes of the initial signal field and the LO, respectively.

In the case of heterodyning with $\omega_s \neq \omega_{LO}$, the intensities of the mix of two harmonic signals contain harmonics oscillating at the difference and the sum frequencies: $\omega_- = \omega_s - \omega_{LO}$ and $\omega_+ = \omega_s + \omega_{LO}$. Since both the optical and the sum frequencies are much larger than the bandwidth of any existing photodiode, the photodetectors are unable to register these high frequency harmonics. Therefore, the output of the balanced detector will be the electrical signal of the difference frequency ω_- that stores the information about the phase of the initial signal [43, 44]. This approach allows detecting two quadrature components at once, since the receiver now does not need to set any phase of the local oscillator. The output photocurrent is given by

$$I(t) = 2R(\lambda)G\sqrt{P_s(t)P_{LO}}\cos(\omega_- t + \Delta\phi). \qquad (3)$$

3.2. Coherent detection with single quadrature selection

In this section we describe the coherent detection scheme with single quadrature selection for the SCW QKD system. We keep the Alice's block identical to the original sender block of the system [24] and change the block of Bob by replacing the single photon detector with the balanced detector (see Fig. 2) [29].

SCW coherent detection is functionally similar to conventional homodyne detection described in the previous section. By contrast to the homodyne detection scheme, as is illustrated in Fig. 3a (3b), the phase modulator in the Bob's module plays the role of the 50/50 beam splitter. After the second modulation the interference is observed at frequencies $\omega_k = \omega + k\Omega$ provided that Alice and Bob use the microwave modulating field with identical frequencies and the phases φ_A and φ_B, respectively. An important point is that the detection result will depend on the phase difference $\Delta\varphi \equiv \varphi_A - \varphi_B$.

In other words, the local oscillator is not used directly as a separate source. SCW homodyning occurs as a result of redistribution of the energy between the intense carrier mode and the weak sidebands, as if a strong coherent beam is mixed with them at a beam splitter. It turns out that the power of subcarrier wave can be either higher or lower than the carrier wave power depending on the phase difference $\Delta\varphi$. These cases of the phase dependent energy redistribution can be interpreted in terms of the interference that might be either constructive or destructive, respectively.

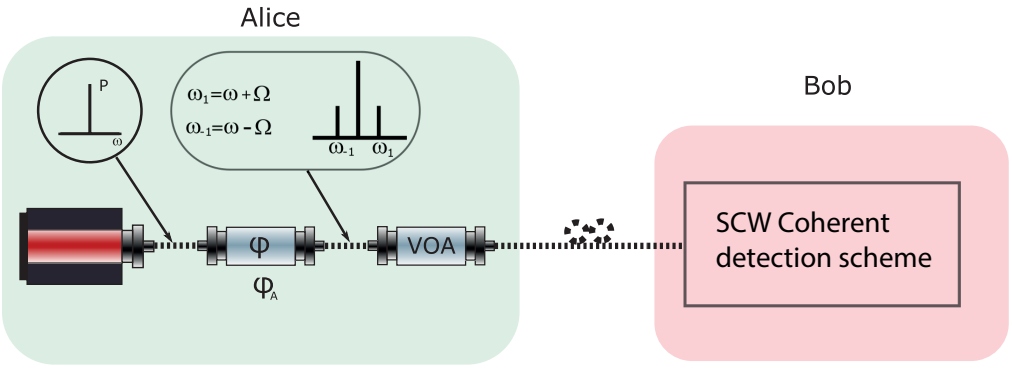

Fig. 2. Principal scheme of SCW CV-QKD setup. The electro-optic phase modulator is denoted by φ; VOA is the variable optical attenuator. Diagrams in circles show the simplified power spectrum.

Our system is calibrated in such way that the differences in power between the sidebands and the carrier mode at $\Delta\varphi = 0$ and $\Delta\varphi = \pi$ are approximately of the same magnitude. A narrow spectral filter then separates the carrier from the sidebands. After that, the sidebands and the central mode are transmitted through the two arms of the balanced detector through the circulator. Finally, the outputs (the carrier and the sidebands) are detected by two different photodiodes, and their photocurrents are subtracted. Thus, one can extract information encoded in the oscillating signal phase. Similar to the conventional homodyne detection in QKD, Bob measures only one quadrature component at a time by selecting the phase of the microwave field from the set of $\varphi_B \in \{0, \pi/2\}$.

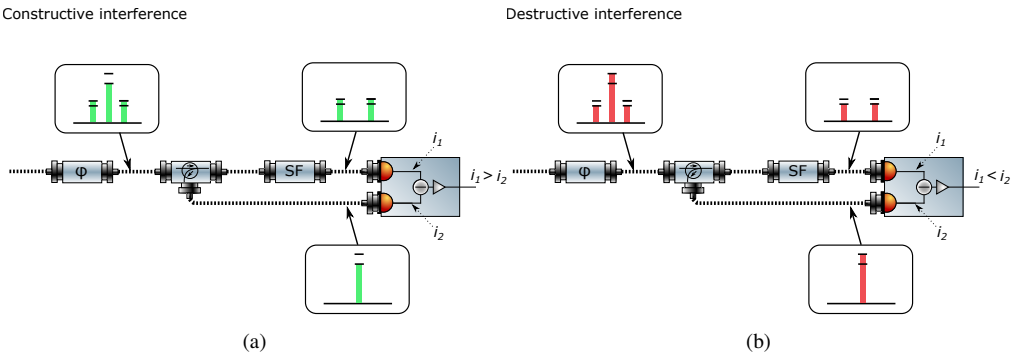

Fig. 3. SCW coherent detection scheme. SF is the spectral filter that cuts off the carrier. The charts show the energy distribution between the carrier and the subcarriers for (a) constructive and (b) destructive interference.

Now we describe a simple classical model (quantum considerations can be found in [29]) of the above homodyne-like coherent detection scheme. The traveling wave phase modulator on the Bob's side generally differs from the Alice's modulator both in the modulation index, $m_B \neq m_A$, and in the phase, $\varphi_B \neq \varphi_A$, thus introducing the phase difference $\Delta\varphi = \varphi_A - \varphi_B$. The expression for the output field emerging after the second modulator $E'(t)$

$$E'(t) = E_0 e^{i\omega t} e^{im_A \cos(\Omega t + \varphi_A)} e^{im_B \cos(\Omega t + \varphi_B)} \tag{4}$$

can be simplified with the help of identities

$$m_A \cos(\Omega t + \varphi_A) + m_B \cos(\Omega t + \varphi_B) = m \cos(\Omega t + \phi), \tag{5a}$$

$$m = \sqrt{m_A^2 + m_B^2 + 2 m_A m_B \cos(\varphi_A - \varphi_B)}, \tag{5b}$$

$$m e^{i\phi} = m_A e^{i\varphi_A} + m_B e^{i\varphi_B}, \tag{5c}$$

where m can be regarded as an effective modulation index describing the wave emerging after two modulators. This index depends on the phase difference $\varphi_A - \varphi_B$, whereas the modulation indices m_A and m_B are both phase independent.

Similar to Eq. (1), the output field can now be written in the form of the Jacobi-Anger expansion:

$$E'(t) = E_0 e^{i\omega t} \sum_{k=-\infty}^{\infty} i^k J_k(m) e^{ik\phi} e^{ik\Omega t} \equiv \sum_{k=-\infty}^{\infty} E_k e^{ik\Omega t}, \quad E_k = E_0 e^{i\omega t} i^{|k|} J_{|k|}(m) e^{ik\phi}. \tag{6}$$

The carrier wave is separated from the sidebands using spectral filtering in the Bob's module For simplicity, we shall neglect the losses and imperfection of the spectral filter. So, we can single out the component at the central frequency to obtain the following expressions for the fields in two arms of the detector

$$E_1(t) = E_0 e^{i\omega t} J_0(m), \quad E_2(t) = \sum_{\substack{k=-\infty, \\ k\neq 0}}^{\infty} E_k e^{ik\Omega t}. \tag{7}$$

Now we can closely follow the line of reasoning leading to Eq. (2), and obtain the time averaged difference of the photocurrents in the form

$$I = R(\lambda) G C \langle |E_2(t)|^2 - |E_1(t)|^2 \rangle_t = R(\lambda) G C E_0^2 (1 - 2J_0^2(m)), \tag{8}$$

where $\langle \ldots \rangle_t = \tau^{-1} \int_0^\tau \ldots \mathrm{d}t$, $\tau = 2\pi/\Omega$. Using temporal averaging assumes that the detectors are insensitive to harmonics of intensities $|E_1(t)|^2$ and $|E_2(t)|^2$ oscillating at radio frequencies. Note that modulation keeps the amplitude of the phase-modulated wave (4) unchanged with $|E'(t)|^2 = E_0^2$, so that Eq. (6) leads to the unitarity condition $\sum_{k=-\infty}^{\infty} J_k^2(m) = 1$ used in derivation of the right-hand side of formula (8).

When the phase difference $\Delta\varphi = \varphi_A - \varphi_B$ is changed, the modulation index m varies between its minimal value $m_{\min} = |m_B - m_A|$ at $\cos(\varphi_A - \varphi_B) = -1$ to the maximal index of modulation $m_{\max} = m_B + m_A$ at $\cos(\varphi_A - \varphi_B) = 1$. In the case where Alice sends non-modulated wave with $m_A = 0$, the output voltage (8) will be zero provided the Bob's index of modulation is adjusted to meet the condition: $J_0(m_B) = 1/\sqrt{2}$ giving $m_B \approx 1.13$.

Figure 4 shows the curves representing dependence of the output voltage on the phase shift φ_A for the in-phase component I and the the quadrature component Q that are computed at $\varphi_B = 0$ and $\varphi_B = \pi/2$, respectively. In our calculations, the parameters are taken to be close to those used in the experiments verifying our model. These are: the carrier wave power is $P_c = 10\ \mu$W; the modulation index of Alice is $m_A = 0.09$; the responsivity of the photodiodes is $R = 0.6$; and the additional gain of the detectors is $G = 4 \times 10^3$.

In order to draw analogy between the proposed scheme and conventional homodyne detection, we assume that the temporally averaged intensities $\langle |E_1(t)|^2 \rangle_t$ and $\langle |E_2(t)|^2 \rangle_t$ of the carrier and the subcarrier waves at the output of Alice's modulator correspond to the amplitudes of the

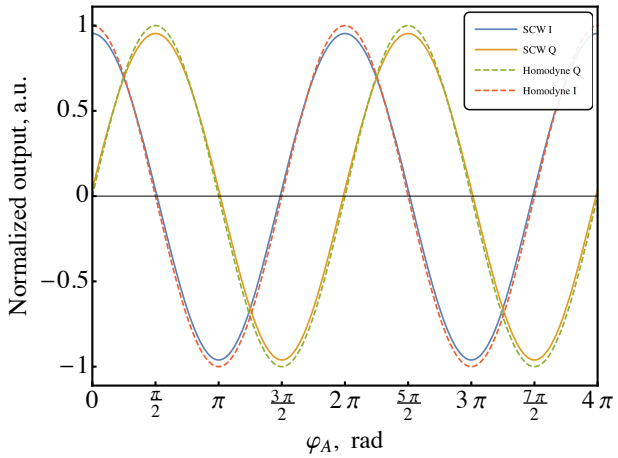

Fig. 4. The in-phase (I) and the quadrature (Q) components of the normalized output signals from the SCW coherent detection scheme (see Eq. (9)) and the classical homodyne scheme.

signal and reference waves: $E_s = E_0\sqrt{1 - J_0^2(m_A)}$ and $E_{LO} = E_0 J_0(m_A)$. Then, for the classical homodyne scheme, the curves for the normalized output (2) $I/I_{\max} = \cos(\Delta\varphi)$ are plotted in Figure 4. It can be seen that the normalized output signal (8) for our scheme

$$I/I_{\max} = \frac{1 - 2J_0^2(m)}{2J_0(m_A)\sqrt{1 - J_0^2(m_A)}} \tag{9}$$

agrees closely with the predicitions of the classical homodyne scheme.

3.3. *Simultaneous selection of both quadrature component*

An important point is that it is possible to construct an optical phase-diversity coherent detection scheme. In this scheme, the receiver is similar to 90° optical hybrid and both the quadrature components can be measured simultaneously. The principal scheme of SCW CV-QKD setup utilizing such a receiver is shown in Figure 5. In this setup, the beam splitter is combined with the two coherent detection schemes where the electro-optic phase modulators are displaced in phase by 90°.

By using the detection scheme depicted in Figure 5, we can measure the two output signals, $E_{1I}(t)$ and $E_{2I}(t)$, from the top arm of the detector with the phase $\varphi_B = 0$, whereas the output signals, $E_{1Q}(t)$ and $E_{2Q}(t)$, from the bottom arm emerge from the detector with the phase $\varphi_B = \pi/2$. Then the output currents after the balanced detectors are converted to the voltages $V_{I,Q}$.

Assuming that the beam splitter dividing the signal in half is ideal and insertion losses are negligible, it is rather straightforward to extend our model presented in the Sec. 3.2 to the case of doubled detection shown in Figure 5. In this case, we can use Eq. (8) to obtain the outputs of the detectors related to quadratures I and Q in the form:

$$I_{I,Q} = \frac{1}{2}R(\lambda)GCE_0^2(1 - 2J_0^2(m_{I,Q})), \tag{10}$$

where $m_I = m|_{\varphi_B=0}$ and $m_Q = m|_{\varphi_B=\pi/2}$. Note, that since this approach introduces additional 3 dB loss at the detection stage, its QKD security should be carefully analyzed.

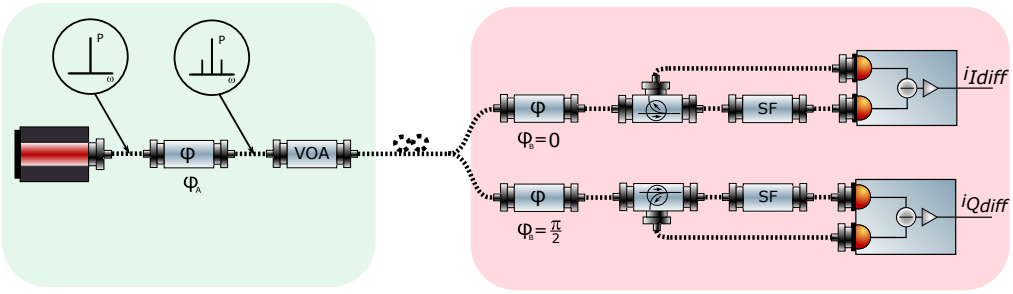

Fig. 5. Principal scheme of SCW CV-QKD setup with phase-diversity coherent receiver.

So, by using these two balanced detectors we can perform simultaneous I/Q measurements. In such measurements, analysis of the experimental results is reduced to obtaining a constellation diagram that will be detailed in Section 4.

3.4. Heterodyne detection

Another well-known method to obtain information about the complex amplitude of the optical fields is heterodyne detection [3, 6, 45–48]. In this section we show how a heterodyne-type detection scheme can be adopted for quadrature phase-coded multimode signals. The mode of operation of our coherent detection scheme demonstrating versatility of the SCW method is described in Figure 6. Note also that such scheme promises significant simplification of implementation.

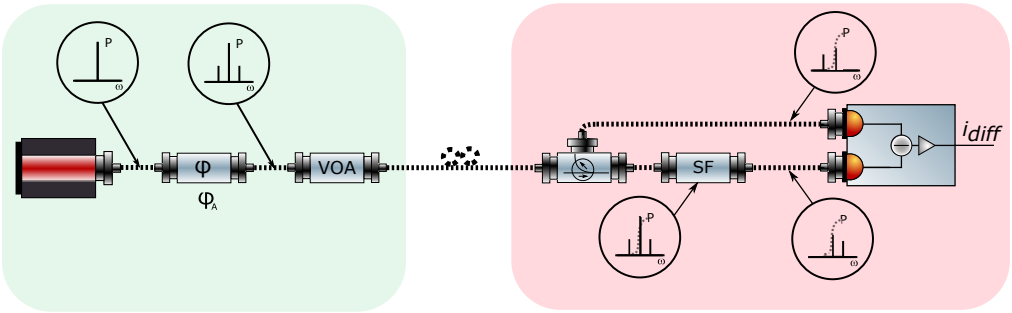

Fig. 6. Principal scheme of SCW CV-QKD setup with heterodyne detection. Examples of power spectra are shown in encircled diagrams and i_{diff} stands for the output photocurrent.

As is shown in Figure 6, similar to the scheme presented in Figure 2, the only component changed in the initial system [24, 25] is the Bob's block whose detection scheme is no longer using the phase modulator. In this scheme spectral filtering is used to mix the carrier wave with the upper and the lower sidebands where subcarrier frequencies are higher and below the carrier frequency ω. For this purpose, the spectral filter bandpass is chosen so as to pass light at the frequency $\omega + \Omega$ and to halve the intensity of the carrier at the frequency ω, whereas the rest of light is reflected back. In other words, the transparency of the spectral filter, T, should meet the conditions: $T(\omega) \approx 0.5$, $T(\omega - \Omega) \to 0$ and $T(\omega + \Omega) \to 1$.

From Eq. (1) we obtain the fields in the separate arms in the following form:

$$E_1(t) = E_0 e^{i\omega t}\Big(\sum_{k=1}^{\infty} i^k J_k(m_A) e^{ik(\Omega t+\varphi_A)} + \sqrt{0.5} J_0(m_A)\Big), \tag{11}$$

$$E_2(t) = E_0 e^{i\omega t}\Big(\sum_{k=1}^{\infty} i^k J_k(m_A) e^{-ik(\Omega t+\varphi_A)} + \sqrt{0.5}J_0(m_A)\Big), \tag{12}$$

where we have used the indentity $J_{-\alpha}(x) = (-1)^{\alpha} J_{\alpha}(x)$ for the Bessel functions. When the modulation index m_A is small, we can apply the lowest order approximation that takes into account only the first order subcarriers

$$E_1(t) \approx E_0\big(iJ_1(m_A)e^{i(\omega_+ t+\varphi_A)} + \sqrt{0.5}J_0(m_A)e^{i\omega t}\big), \tag{13}$$

$$E_2(t) \approx E_0\big(iJ_1(m_A)e^{i(\omega_- t-\varphi_A)} + \sqrt{0.5}J_0(m_A)e^{i\omega t}\big), \tag{14}$$

where $\omega_{\pm} = \omega \pm \Omega$, and derive the output photocurrent in the absence of noise

$$I(t) = R(\lambda)GC(|E_2(t)|^2 - |E_1(t)|^2) = R(\lambda)GC2\sqrt{2}E_0^2 J_0(m_A)J_1(m_A)\sin(\Omega t + \varphi_A). \tag{15}$$

Clearly, this result bears a striking resemblance to the classical heterodyning.

As in the previous section, we now discuss this analogy using Eq. (3) with ω and $\Delta\varphi$ replaced by Ω and $\varphi_A + \pi/2$, respectively. For this purpose, we assume that the amplitudes of the signal and reference waves are $E_s = E_0\sqrt{1 - J_0^2(m_A)}$ and $E_{LO} = E_0 J_0(m_A)$ and compare the output of the classical heterodyne, $I_{\max}\sin(\Omega t + \varphi_A)$, with the signal given in Eq. (15). Figure 7 shows that the normalized output of our scheme

$$I(t)/I_{\max} = \frac{\sqrt{2}J_1(m_A)}{\sqrt{1 - J_0^2(m_A)}}\sin(\Omega t + \varphi_A) \tag{16}$$

turns out to be very close to the output of the classical scheme. It should be stressed that, in this analysis, the detectors are assumed to be sensitive to the radio frequency Ω.

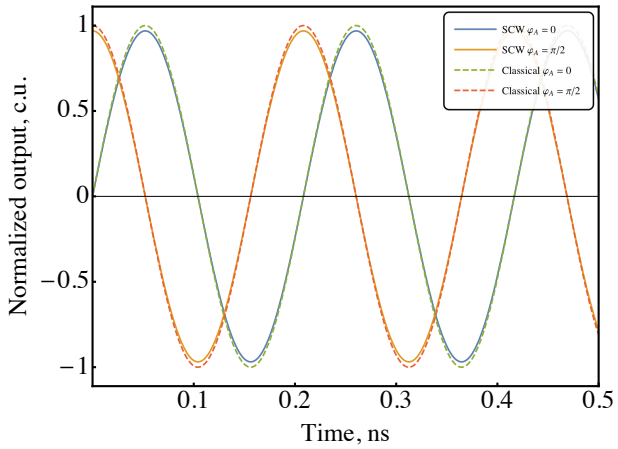

Fig. 7. Time dependence of the normalized heterodyne-derived signals for the SCW and the classical detection schemes.

Demodulation of the received signal can be carried out by standard telecommunication methods using a quadrature synchronous demodulator [6, 49–52]. The demodulator setup allows one to observe the in-phase (initial) and quadrature (shifted by $\pi/2$ using a voltage generator) signal components simultaneously on the analyzer and thus extract the information on the phase selected by Alice.

The main disadvantage of this method is the need to find a balance between the capabilities of spectral filters and balanced detectors. On the one hand, an increase of modulation frequency Ω leads to the growth of required detector's bandwidth, what results in extra electronic noises [53]. Usually bandwidth of balanced detectors used for quantum measurements is less than 1 GHz [54]. On the other hand, low modulation frequencies perplex subcarriers' spectral filtering. Thus one of the main challenges for practical implementation of such scheme is to find an optimal modulation frequency that satisfies both of these conditions.

4. Experimental results

In this section we present the results of our experiments verifying the theoretical models presented in the previous section. For the homodyne-like detection setup shown in Figure 2, our proof-of-principle experiment have used a 1550 nm 10 μW fiber-coupled laser directed into the $LiNbO_3$ electro-optic phase modulator with the electrical signal frequency $\Omega = 4.8$ GHz. The modulation index m_B is adjusted to maximize the difference between the results for different values of $\Delta\varphi$ and the phase dependence of the output voltage is expected to be nearly harmonic (see Figure 4). After the second modulation the spectral components are transmitted through the circulator to a fiber Bragg grating spectral filter. In the core of the fiber Bragg grating filter the refractive index periodically changes in the longitudinal direction, and the spectral selectivity of reflection from fiber Bragg gratings is due to diffraction by periodic optical inhomogeneities. The sideband components are transmitted through the filter to the first arm. The filter reflects the component at the central frequency back to the circulator. After passing the circulator, the reflected carrier wave propagates in the second arm of the balanced detector. The two output ports of the circulator are coupled to the input ports of a self-developed balanced detector (the measurement bandwidth is 100 MHz, the gain is $G = 4 \cdot 10^3$ and the responsivity is $R = 0.6$).

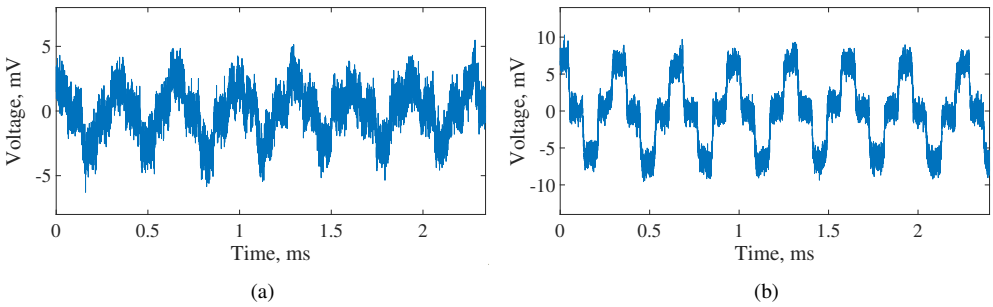

Fig. 8. Time dependence of the output voltage for the homodyne-like coherent detection scheme shown in Fig. 2. The extreme points correspond to the constructive and destructive interference. The phase difference $\Delta\varphi$ varies periodically in time switching between the values from a discrete set: $\{0, \pi/2, \pi, 3\pi/2\}$. Two cases are shown: (a) $P_c = 9.96$ μW, $P_s = 40.00$ nW; and (b) $P_c = 9.5$ μW, $P_s = 500.00$ nW.

Figure 8 presents the output voltage measured in relation of time when the phase difference (the phase φ_A is set to be zero), $\Delta\varphi$, undergoes time-periodic piecewise changes between the states with equidistant values from a discrete set $\{0, \pi/2, \pi, 3\pi/2\}$. Referring to Fig. 8a, it can be seen that, in the case where the carrier wave power after the modulation was $P_c = 9.96$ μW and the total power of the subcarriers was $P_s = 40.00$ nW, variations of the voltage level are almost indiscernible. By contrast, Figure 8b demonstrates the case with unambiguously distinguishable voltage levels that occurs at $P_c = 9.5$ μW and $P_s = 500.00$ nW. Thus, our coherent detection scheme is sufficiently sensitive to estimate the phase of the quadrature phase-coded multimode signals from the electro-optic phase modulator.

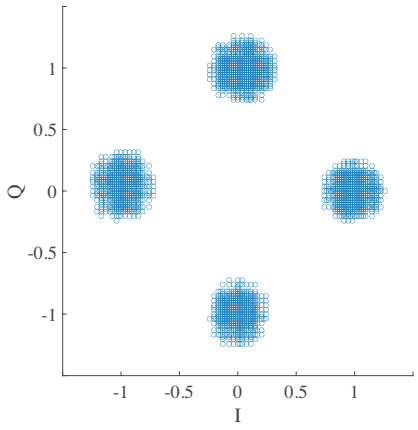

Fig. 9. 4-PSK constellation diagram recovered from the phase-modulated optical signal, P_c = 9.5 μW, P_s = 500.00 nW.

We have also performed the experiment for the optical phase-diversity coherent receiver sketched in Figure 5. The 4-PSK constellation diagram recovered from the phase-modulated optical signal using the optical phase-diversity coherent receiver is depicted in Figure 9.

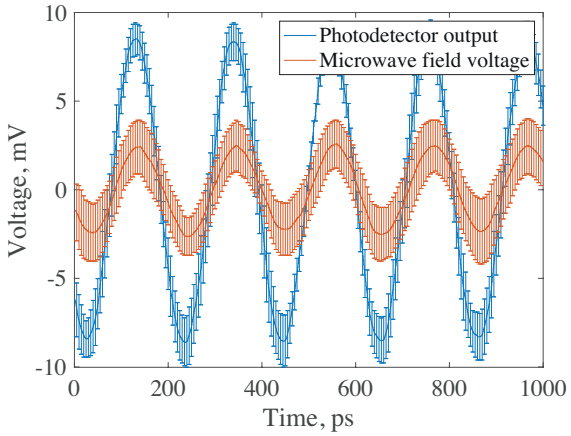

Fig. 10. Time dependence of microwave field voltage and the output voltage for balanced detector's single arm (P_c = 225.00 μW, P_s = 146.50 μW) using the SCW heterodyning. Mean values are indicated along with standard deviations.

In order to test the heterodyne scheme (see Figure 6), we need to get around the above-mentioned difficulties concerning the frequency bandwidth. For this purpose, we have utilized the photodetector with 6.17 GHz bandwidth in the single arm of the scheme described in Figure 6 to obtain the signal at the intermediate frequency. The measured curves for the output voltage and the microwave field are presented in Figure 10. The results show that the signal light is down-converted to the intermediate frequency coincident with the frequency of the microwave field used in the electro-optic phase modulator.

5. Conclusion

In this paper we have applied several approaches to put coherent detection schemes into the framework of the subcarrier wave QKD systems. In our homodyne-like coherent detection schemes (see Sec. 3.2 and Sec. 3.3), the phase-modulated light emerging from the Bob's modulator is splitted into the carrier and the subcarrier waves and the output signal is determined by the difference between the responses of the photodiodes to the light of these two waves. By contrast, in our heterodyne-type detection scheme described in Sec. 3.4 the light modulated by Alice is directly used as the input wave. This wave, similar to the homodyne-like scheme, is divided into two waves. But, in contrast to this scheme, these waves are obtained by filtering out either the lower or the upper sidebands. In this case, we have shown that the differential signal which is oscillating with the microwave frequency can be used to extract the information about the phase encoded by Alice.

In our theoretical considerations we have presented simple classical models emphasizing the analogy between the suggested coherent detection schemes and the standard homodyne/heterodyne methods. Interestingly, quantum considerations of our previous work [29] being necessary to perform security analysis can be related to the classical approach presented in Sec. 3.2. To this end, we begin with the modulated quantum state after Bob's modulator written in the form (see Ref. [34] for details)

$$|\Psi\rangle = V|\alpha_{\rm in}\rangle = \otimes_{\nu=-S}^{S}|\alpha_\nu\rangle \equiv |\alpha_0\rangle \otimes |\boldsymbol{\alpha}\rangle_{SB}, \tag{17}$$

$$\alpha_\nu = M^*_{\nu 0}\alpha_{\rm in}, \quad |\boldsymbol{\alpha}\rangle_{SB} = \otimes_{\nu\neq 0}|\alpha_\nu\rangle, \tag{18}$$

where $|\alpha_{\rm in}\rangle$ is the input coherent state of the Alice's modulator and the matrix elements of the evolution operator $M_{\nu 0}$ are described in [34] and, in the large S limit, are given by

$$|M_{\nu 0}(\beta)|^2 \approx J^2_\nu(m), \quad m^2 \approx m_A^2 + m_B^2 + 2m_A m_B\cos(\varphi_A - \varphi'_B), \quad \varphi'_B = \varphi_B - \varphi_0. \tag{19}$$

Following the line of reasoning presented in Refs. [55, 56], it can be shown that the difference of photocounts follows the Skellam distribution

$$P(k) = {\rm e}^{-\mu_{SB}-\mu_0}\left(\frac{\mu_{SB}}{\mu_0}\right)^k I_{|k|}(2\sqrt{\mu_0\mu_{SB}}), \quad k = k_{SB} - k_0 \in \mathbb{Z},$$

$$\mu_0 = \xi|\alpha_0|^2, \quad \mu_{SB} = \sum_{\nu\neq 0}\xi_\nu|\alpha_\nu|^2, \tag{20}$$

where I_k is the k-order modified Bessel function of the first kind; ξ_μ is the efficiency of the photodetector for the μth mode (for simplicity, we shall assume that the efficiency is independent of μ so that $\xi_\mu = \xi$). It is known that, under certain conditions, the above distribution can be approximated by the normal (Gaussian) distribution

$$P(k) \approx \frac{1}{\sqrt{2\pi\sigma^2}}\exp\left(-\frac{(k-\langle k\rangle)^2}{2\sigma^2}\right), \tag{21}$$

determined by the mean value

$$\langle k\rangle = \mu_{SB} - \mu_0 = \xi(1 - 2|M_{00}|^2)|\alpha_{\rm in}|^2, \tag{22}$$

and the variance

$$\sigma^2 = \mu_{SB} + \mu_0 = \xi|\alpha_{\rm in}|^2. \tag{23}$$

When $|M_{00}|^2 \approx J_0^2(m)$, we arrive at the conclusion that the mean value $\langle k\rangle$ is proportional to the difference of photocurrents given by Eq. (8).

Our experimental results clearly demonstrate practical feasibility of the presented detection schemes. Futher development will require a more sophisticated and detailed analysis of these schemes using the methods of quantum optics. This will allow their legitimate employment in quantum computing, quantum cryptography, and quantum tomography. The concluding remark is that our continuous variable version of the SCW method can be regarded as an alternative to the method suggested in [30] and, in addition,the CV-SCW approach was recently demonstrated to be useful for designing quantum random number generators [57].

Acknowledgements

This work was funded by Government of Russian Federation (Grant No. MK-777.2020.8).

Disclosures

The authors declare no conflicts of interest.

References

1. L. I. Anderson, *Nicola Tesla: Lecture Before the New York Academy of Sciences - April 6, 1897* (Twenty First Century Books, 1994).
2. B. Roger and H. Georges, "Double heterodyne radio receiver," (1952). US Patent 2,606,285.
3. V. V. Protopopov, *Laser Heterodyning* (Springer Berlin Heidelberg, 2009).
4. D.-S. Ly-Gagnon, S. Tsukamoto, K. Katoh, and K. Kikuchi, "Coherent detection of optical quadrature phase-shift keying signals with carrier phase estimation," J. Light. Technol. **24**, 12 (2006).
5. S. Tanosaki, Y. Sasaki, M. Takagi, A. Ishikawa, H. Inage, R. Emori, J. Suzuki, T. Yuasa, H. Taniguchi, B. Devaraj *et al.*, "In vivo laser tomographic imaging of mouse leg by coherent detection imaging method," Opt. Rev. **10**, 447–451 (2003).
6. K. Kikuchi, "Fundamentals of coherent optical fiber communications," J. Light. Technol. **34**, 157–179 (2015).
7. A. Mecozzi and M. Shtaif, "Coherent detection with an incoherent local oscillator," Opt. Express **26**, 33970–33981 (2018).
8. Y. Lu, T. Zhu, L. Chen, and X. Bao, "Distributed vibration sensor based on coherent detection of phase-OTDR," J. Light. Technol. **28**, 3243–3249 (2010).
9. H. P. Yuen and V. W. Chan, "Noise in homodyne and heterodyne detection," Opt. Lett. **8**, 177–179 (1983).
10. A. Barchielli, "Direct and heterodyne detection and other applications of quantum stochastic calculus to quantum optics," Quantum Opt. J. Eur. Opt. Soc. Part B **2**, 423 (1990).
11. S. Wallentowitz and W. Vogel, "Unbalanced homodyning for quantum state measurements," Phys. Rev. A **53**, 4528 (1996).
12. F. Grosshans, G. Van Assche, J. Wenger, R. Brouri, N. J. Cerf, and P. Grangier, "Quantum key distribution using gaussian-modulated coherent states," Nature **421**, 238–241 (2003).
13. T. Hirano, H. Yamanaka, M. Ashikaga, T. Konishi, and R. Namiki, "Quantum cryptography using pulsed homodyne detection," Phys. Rev. A **68**, 042331 (2003).
14. A. Leverrier and P. Grangier, "Continuous-variable quantum-key-distribution protocols with a non-gaussian modulation," Phys. Rev. A **83**, 042312 (2011).
15. M. Heid and N. Lütkenhaus, "Efficiency of coherent-state quantum cryptography in the presence of loss: Influence of realistic error correction," Phys. Rev. A **73**, 052316 (2006).
16. K. Brádler and C. Weedbrook, "Security proof of continuous-variable quantum key distribution using three coherent states," Phys. Rev. A **97**, 022310 (2018).
17. P. Papanastasiou, C. Lupo, C. Weedbrook, and S. Pirandola, "Quantum key distribution with phase-encoded coherent states: Asymptotic security analysis in thermal-loss channels," Phys. Rev. A **98**, 012340 (2018).
18. S. Ghorai, P. Grangier, E. Diamanti, and A. Leverrier, "Asymptotic security of continuous-variable quantum key distribution with a discrete modulation," Phys. Rev. X **9**, 021059 (2019).
19. J. Lin, T. Upadhyaya, and N. Lütkenhaus, "Asymptotic security analysis of discrete-modulated continuous-variable quantum key distribution," Phys. Rev. X **9**, 041064 (2019).
20. G. Zhang, J. Haw, H. Cai, F. Xu, S. Assad, J. Fitzsimons, X. Zhou, Y. Zhang, S. Yu, J. Wu *et al.*, "An integrated silicon photonic chip platform for continuous-variable quantum key distribution," Nat. Photonics **13**, 839–842 (2019).
21. Y. Zhang, Z. Chen, S. Pirandola, X. Wang, C. Zhou, B. Chu, Y. Zhao, B. Xu, S. Yu, and H. Guo, "Long-distance continuous-variable quantum key distribution over 202.81 km of fiber," Phys. Rev. Lett. **125**, 010502 (2020).
22. J.-M. Merolla, Y. Mazurenko, J.-P. Goedgebuer, H. Porte, and W. T. Rhodes, "Phase-modulation transmission system for quantum cryptography," Opt. Lett. **24**, 104–106 (1999).
23. J. Mora, A. Ruiz-Alba, W. Amaya, A. Martínez, V. García-Muñoz, D. Calvo, and J. Capmany, "Experimental demonstration of subcarrier multiplexed quantum key distribution system," Opt. Lett. **37**, 2031–2033 (2012).

24. A. Gleim, V. Egorov, Y. V. Nazarov, S. Smirnov, V. Chistyakov, O. Bannik, A. Anisimov, S. Kynev, A. Ivanova, R. Collins *et al.*, "Secure polarization-independent subcarrier quantum key distribution in optical fiber channel using BB84 protocol with a strong reference," Opt. Express **24**, 2619–2633 (2016).
25. G. Miroshnichenko, A. Kozubov, A. Gaidash, A. Gleim, and D. Horoshko, "Security of subcarrier wave quantum key distribution against the collective beam-splitting attack," Opt. Express **26**, 11292–11308 (2018).
26. A. Gaidash, A. Kozubov, and G. Miroshnichenko, "Methods of decreasing the unambiguous state discrimination probability for subcarrier wave quantum key distribution systems," JOSA B **36**, B16–B19 (2019).
27. V. Chistiakov, A. Kozubov, A. Gaidash, A. Gleim, and G. Miroshnichenko, "Feasibility of twin-field quantum key distribution based on multi-mode coherent phase-coded states," Opt. Express **27**, 36551–36561 (2019).
28. S. M. Kynev, V. V. Chistyakov, S. V. Smirnov, K. P. Volkova, V. I. Egorov, and A. V. Gleim, "Free-space subcarrier wave quantum communication," J. Physics: Conf. Ser. **917**, 052003 (2017).
29. E. Samsonov, R. Goncharov, A. Gaidash, A. Kozubov, V. Egorov, and A. Gleim, "Subcarrier wave continuous variable quantum key distribution with discrete modulation: mathematical model and finite-key analysis," Sci. Reports **10**, 10034 (2020).
30. J. Fang, P. Huang, and G. Zeng, "Multichannel parallel continuous-variable quantum key distribution with gaussian modulation," Phys. Rev. A **89**, 022315 (2014).
31. L. Gyongyosi and S. Imre, "Subcarrier domain of multicarrier continuous-variable quantum key distribution," J. Stat. Phys. **177**, 960–983 (2019).
32. Y. Wang, Y. Mao, W. Huang, D. Huang, and Y. Guo, "Optical frequency comb-based multichannel parallel continuous-variable quantum key distribution," Opt. Express **27**, 25314–25329 (2019).
33. S. Haykin, *Communication systems* (John Wiley & Sons, 2008).
34. G. P. Miroshnichenko, A. D. Kiselev, A. I. Trifanov, and A. V. Gleim, "Algebraic approach to electro-optic modulation of light: exactly solvable multimode quantum model," JOSA B **34**, 1177–1190 (2017).
35. J. Capmany and C. R. Fernández-Pousa, "Quantum model for electro-optical phase modulation," JOSA B **27**, A119–A129 (2010).
36. P. Kumar and A. Prabhakar, "Evolution of quantum states in an electro-optic phase modulator," IEEE J. Quantum Electron. **45**, 149–156 (2008).
37. A. Yariv and P. Yeh, *Optical waves in crystals*, vol. 5 (Wiley New York, 1984).
38. N. G. Gonzalez, D. Zibar, X. Yu, and I. T. Monroy, "Optical phase-modulated radio-over-fiber links with k-means algorithm for digital demodulation of 8psk subcarrier multiplexed signals," in *Optical Fiber Communication Conference,* (Optical Society of America, 2010), p. OML3.
39. I. Gasulla and J. Capmany, "Phase-modulated radio over fiber multimode links," Opt. Express **20**, 11710–11717 (2012).
40. Y. Zhang, K. Xu, R. Zhu, J. Li, J. Wu, X. Hong, and J. Lin, "Photonic dpask/qam signal generation at microwave/millimeter-wave band based on an electro-optic phase modulator," Opt. Lett. **33**, 2332–2334 (2008).
41. T. Hirano, T. Ichikawa, T. Matsubara, M. Ono, Y. Oguri, R. Namiki, K. Kasai, R. Matsumoto, and T. Tsurumaru, "Implementation of continuous-variable quantum key distribution with discrete modulation," Quantum Sci. Technol. **2**, 024010 (2017).
42. A. Leverrier, "Theoretical study of continuous-variable quantum key distribution," Ph.D. thesis, Télécom ParisTech (2009).
43. M. Yoshida, H. Goto, K. Kasai, and M. Nakazawa, "64 and 128 coherent qam optical transmission over 150 km using frequency-stabilized laser and heterodyne pll detection," Opt. Express **16**, 829–840 (2008).
44. J. Hongo, K. Kasai, M. Yoshida, and M. Nakazawa, "1-Gsymbol/s 64-QAM coherent optical transmission over 150 km," IEEE Photonics Technol. Lett. **19**, 638–640 (2007).
45. H. Gebbie, N. Stone, E. Putley, and N. Shaw, "Heterodyne detection of sub-millimetre radiation," Nature **214**, 165–166 (1967).
46. A. Maznev, K. Nelson, and J. A. Rogers, "Optical heterodyne detection of laser-induced gratings," Opt. Lett. **23**, 1319–1321 (1998).
47. D. L. Fried, "Optical heterodyne detection of an atmospherically distorted signal wave front," Proc. IEEE **55**, 57–77 (1967).
48. O. DeLange, "Optical heterodyne detection," IEEE Spectr. **5**, 77–85 (1968).
49. M. Bylina, S. Glagolev, and A. Diubov, "Comparative analysis of direct and coherent detection methods for digital information optical signals. Part 2. Coherent detection," Proc. Telecommun. Univ. **3**, 21–28 (2017).
50. C. Wang, Y. Qu, and Y. P. T. Tang, "IQ quadrature demodulation algorithm used in heterodyne detection," Infrared Phys. & Technol. **72**, 191–194 (2015).
51. R. Bohme and M. Eichin, "Heterodyne receiver with synchronous demodulation for receiving time signals," (1999). US Patent 5,930,697.
52. Y.-K. Chen, U.-V. Koc, and A. Leven, "Optical heterodyne receiver and method of extracting data from a phase-modulated input optical signal," (2010). US Patent 7,650,084.
53. Y.-M. Chi, B. Qi, W. Zhu, L. Qian, H.-K. Lo, S.-H. Youn, A. Lvovsky, and L. Tian, "A balanced homodyne detector for high-rate gaussian-modulated coherent-state quantum key distribution," New J. Phys. **13**, 013003 (2011).
54. X. Tang, R. Kumar, S. Ren, A. Wonfor, R. Penty, and I. White, "Performance of continuous variable quantum key distribution system at different detector bandwidth," Opt. Commun. p. 126034 (2020).

55. W. Vogel and J. Grabow, "Statistics of difference events in homodyne detection," Phys. Rev. A **47**, 4227 (1993).
56. M. Bina, A. Allevi, M. Bondani, and S. Olivares, "Homodyne-like detection for coherent state-discrimination in the presence of phase noise," Opt. Express **25**, 10685–10692 (2017).
57. E. Samsonov, B. Pervushin, A. Ivanova, A. Santev, V. Egorov, S. Kynev, and A. Gleim, "Vacuum-based quantum random number generator using multi-mode coherent states," Quantum Inf. Process. **19**, 1–11 (2020).